Integrated analysis of anatomical and electrophysiological human intracranial data

Arjen Stolk [1,2*], Sandon Griffin[1], Roemer van der Meij[3], Callum Dewar[1,4], Ignacio Saez[1], Jack J. Lin[5], Giovanni Piantoni [6], Jan-Mathijs Schoffelen [2], Robert T. Knight[1,7] and Robert Oostenveld [2,8]

Human intracranial electroencephalography (iEEG) recordings provide data with much greater spatiotemporal precision than is possible from data obtained using scalp EEG, magnetoencephalography (MEG), or functional MRI. Until recently, the fusion of anatomical data (MRI and computed tomography (CT) images) with electrophysiological data and their subsequent analysis have required the use of technologically and conceptually challenging combinations of software. Here, we describe a comprehensive protocol that enables complex raw human iEEG data to be converted into more readily comprehensible illustrative representations. The protocol uses an open-source toolbox for electrophysiological data analysis (FieldTrip). This allows iEEG researchers to build on a continuously growing body of scriptable and reproducible analysis methods that, over the past decade, have been developed and used by a large research community. In this protocol, we describe how to analyze complex iEEG datasets by providing an intuitive and rapid approach that can handle both neuroanatomical information and large electrophysiological datasets. We provide a worked example using an example dataset. We also explain how to automate the protocol and adjust the settings to enable analysis of iEEG datasets with other characteristics. The protocol can be implemented by a graduate student or postdoctoral fellow with minimal MATLAB experience and takes approximately an hour to execute, excluding the automated cortical surface extraction.

Introduction

iEEG enables simultaneous recordings from tens to hundreds of electrodes placed directly on the neocortex (electrocorticography (ECoG)), or intracortically (stereoelectroencephalography (SEEG)). In humans, iEEG is most commonly used in surgery on medication-refractory epilepsy patients because noninvasive techniques such as scalp EEG and MRI do not provide sufficient information to guide the surgery. Each electrode reflects the activity of tens of thousands of neurons[1,2], thus, the recording and stimulation of these neural populations facilitates the identification of epileptogenic tissue and the mapping of functional areas of human cortex to guide neurosurgery. The outcome of these procedures can be directly observed when the neural or behavioral response is straightforward, such as speech arrest or muscle movement with direct stimulation[3]. However, a more complex empirical study requires accurate knowledge of the location of the electrode and the part of the brain from which the local electrophysiological signal has originated. This integrated information is key when undertaking basic and clinical research work aimed at understanding human neural and cognitive processing[4,5].

Human iEEG analysis has traditionally relied on stand-alone and ad hoc workflows that separately analyze anatomical and functional aspects of iEEG data. This has meant that research laboratories must assemble software combinations to convert file formats (e.g., "DICOM (Digital Imaging and Communications in Medicine) to NIfTI (Neuroimaging Informatics Technology Initiative)" using MRIConvert), co-register anatomical scans (e.g., CT to MRI using SPM[6], FSL[7], or AFNI[8]), localize electrodes (e.g., BioImage Suite[9]), and sort and label electrodes to match the format of the functional recording file (manually or using custom software) in order to process the neuroanatomical data. More efficient workflows for localizing and visualizing electrodes have been developed[10–17]; however,

[1]Helen Wills Neuroscience Institute, University of California, Berkeley, Berkeley, CA, USA. [2]Donders Institute for Brain, Cognition, and Behaviour, Radboud University, Nijmegen, The Netherlands. [3]Department of Cognitive Science, University of California, San Diego, La Jolla, CA, USA. [4]College of Medicine, University of Illinois, Chicago, IL, USA. [5]Department of Neurology, University of California, Irvine, Irvine, CA, USA. [6]Department of Neurology, Massachusetts General Hospital and Harvard Medical School, Boston, MA, USA. [7]Department of Psychology, University of California, Berkeley, Berkeley, CA, USA. [8]NatMEG, Karolinska Institutet, Stockholm, Sweden. *e-mail: astolk@berkeley.edu

Box 1 | Getting started with FieldTrip ● Timing ~1 min

All the protocol code is directly integrated with and freely available through FieldTrip[55]. This MATLAB-based open-source toolbox offers advanced analysis methods for electrophysiological data, such as event-related averaging, frequency and time–frequency analysis, source modeling (for EEG and MEG), connectivity analysis, classification, real-time data processing, and (non)parametric statistical inference. The implementation as a toolbox allows users to perform elaborate and structured analyses of large datasets using the MATLAB command line and batch scripting. Tutorial documentation, answers to frequently asked questions, and example code are available online at http://www.fieldtriptoolbox.org. The toolbox's infrastructure allows users and developers to relatively easily extend the functionality and implement new algorithms. Over the past decade, the FieldTrip toolbox user base has grown to an estimated 5000 researchers.

To get started with FieldTrip, download the most recent version from its homepage or GitHub, and set up your MATLAB path using the command below:

```
addpath <path to fieldtrip home directory>
ft_defaults
```

FieldTrip functionalities, recognizable by an `ft` prefix, typically have a single output argument and one or two input arguments, the first input argument being configuration structure, `cfg`. See some example code below:

```
cfg = [];
cfg.hpfilter = 'yes';
cfg.hpfreq = 1;
data_filt = ft_preprocessing(cfg, data);
```

In this example, input data are processed by `ft_preprocessing` according to the parameters specified in the `cfg` fields, in this case applying a 1-Hz high-pass filter. Each function's optional parameters are available in the respective function's header (type `help functionname`) and examples are provided on the wiki.

The `cfg` structure that holds the parameters to the algorithm at the present level is automatically appended to the output data structure, i.e., `data_filt.cfg`. Configuration structures used at previous levels are kept in data_filt.cfg.previous, data_filt.cfg.previous.previous, and so on. This nesting of previous configurations allows for access to the full data provenance at any level of the analysis pipeline (type `help ft_analysispipeline` for how to visualize the pipeline as a flowchart).

a single software package to allow researchers to efficiently process the anatomical data within a single work environment, and seamlessly fuse with the electrophysiological data and its subsequent analysis, is a preferable solution. In addition to the benefits of a single software package, any software must enable the processing of raw data into results and illustrative representations to be completely transparent in order to enable a convenient and reliable exchange of data and workflows between researchers[18]. These two qualities are particularly important, given that the research field is growing, the analysis of the data is complex, and the gold standard for data analysis has yet to be defined.

Here, we describe how to implement a comprehensive protocol that integrates anatomical and functional human iEEG analysis. In addition to efficiently combining and expanding the functionalities of existing software[6–17], the present protocol provides tools that enable anatomically informed data exploration and representation of iEEG data. The protocol is integrated with the MATLAB-based open-source FieldTrip toolbox (Box 1), which enables users to build on a continuously growing set of analysis techniques already used by a large research community. The data formats used by most popular electrophysiological data–acquisition systems can be used by the FieldTrip toolbox, and the analysis code builds on other software packages such as SPM and EEGLAB[19]. In contrast to the host of proprietary programs currently available for the analysis of electrophysiological data, a major rationale for the development of FieldTrip was to provide complete transparency, in order to promote a deeper understanding of the analysis techniques and, hence, enhance the quality of the scientific work that depends on these techniques. Accordingly, all computer code is fully accessible and the well-defined data structures contain full details to facilitate sharing between researchers. Our aim is to use these open-source features to advance the field of human iEEG by promoting interaction within and across methodologically contiguous research areas (e.g., noninvasive electrophysiology such as EEG or MEG).

Applications of the protocol

This protocol is particularly useful when studying human neural and cognitive processes with iEEG because human iEEG analysis requires the handling of large neuroanatomical and electrophysiological datasets. A wide range of basic and clinical studies use iEEG, including studies of higher-order cognition[20,21] and those involving the localization and understanding of the sources and features of epileptogenic activity[22,23]. The methodological challenges that iEEG researchers face can be grouped

into either obstacles that are common to most empirical work or obstacles that are study-specific. This protocol aims to facilitate the resolution of the former while also providing guidance and flexibility that enable study-specific obstacles to be overcome. As an example of the types of data this protocol can be applied to, the protocol we describe here has been used previously to perform group-level investigations of emotion- and language-related neural dynamics and connectivity of the human hippocampus[20,24].

Advantages and limitations of the protocol

The main advantages of our protocol are that it (i) guides the researcher from the multitude of raw intracranial data files to integrated observations, in a fast and efficient way; (ii) is directly integrated with a comprehensive and open-source hub for electrophysiological data analysis; (iii) can be readily adapted and automated; (iv) is completely transparent; and (v) produces reproducible workflows and datasets that can be easily shared and generalized to other research modalities. The main limitation is that the MATLAB command-line interface requires some basic programming knowledge, which may require more initial learning as compared with the execution of computer commands through a (black box) graphical user interface. However, the use of computer commands can be relatively easily mastered by following this protocol, enabling the use of batch scripting to efficiently deal with repeated analyses within and across subjects. In addition, using computer commands ultimately enables a deeper understanding of the underlying algorithms.

Human intracranial datasets come in different sizes and shapes, and can be processed for different purposes, making it important for a protocol to strike the right balance between efficiency and flexibility. This need is further amplified by the relatively unique nature of intracranial data, typically imposing greater demands on alternative options and strategies in the analysis than noninvasive data recorded with more standardized hardware and software in dedicated laboratory settings. In addition to providing a quick guide to interpretable results, our protocol allows easy switching between analysis methods to accommodate the processing of data from different cases and situations. By changing a single parameter at execution, one can, for instance, readily apply a different fusion cost function or filter setting. The well-defined data structures created by the protocol contain full processing details at any level of the analysis pipeline, enabling researchers to adapt to circumstances by selecting between the processing algorithms in a transparent and reproducible way.

The spatiotemporal precision of iEEG provides a unique window on neural processing. The size and dimensions of this window, however, may grow disproportionally large with certain types of analyses, complicating the overall interpretability of the data. Starting from the two dimensions of the raw neural signal (channels and time), a time–frequency analysis, for instance, results in three dimensions in the output (power as a function of channel, time, and frequency), whereas between-channel connectivity analysis expands the combinatorial space to four dimensions. Our protocol enables the interactive manipulation of anatomically informed graphical representations of the neural data, which facilitates visualization of the multidimensional outcome of an iEEG analysis.

Integration with FieldTrip

In addition to the complete transparency that comes with an open-source toolbox, the integration with FieldTrip enables iEEG researchers to build on algorithms for reading raw data in various formats, data preprocessing, event-related potential analysis, spectral analysis, source modeling, connectivity analysis, classification, real-time data processing, and statistical inference. When applied to human iEEG data, these methods allow characterization of neural information flow with a level of detail inaccessible to noninvasive techniques. In addition, invasive and noninvasive human electrophysiology can be visualized together using very similar analysis pipelines to enable an integrated presentation of neural processing or a comparison of MEG/EEG source reconstruction methods with iEEG.

The open-source development model allows for additional components to be relatively easily added to the protocol. For example, several techniques exist to compensate for electrode displacement due to the 'brain-shift' phenomenon explained below[11,12,25–32]. Each of these techniques has different strengths and weaknesses; thus, the best technique to use can be determined on a case-by-case basis. FieldTrip's modular architecture enables developers to incorporate new techniques and users to subsequently utilize these techniques by changing a single parameter at function call. This facilitates the use of the protocol in new research areas, including single- and multi-unit recordings, 'NeuroGrid' recordings[33], wireless 'Neural Dust' recordings[34], (deep) brain stimulation[35,36], and

multimodal imaging[12]. We plan to coordinate with these new electrophysiological endeavors and to continue sharing analysis code with other software packages.

### Compatibility with FreeSurfer

The protocol is compatible with the freely available FreeSurfer software package[37]. Although optional, processing of the anatomical MRI with FreeSurfer (Step 6) offers several advantages for subsequent analysis and data interpretation. Processing the MRI with FreeSurfer results in the creation of a cortical mesh, consisting of approximately equally sized triangles that form a topological sphere for each of the cerebral hemispheres. This cortical mesh enables an anatomically realistic representation of the electrophysiological data on the neocortex (e.g., bottom center in Fig. 1). A smoothed version of the extracted cortical surface can be used to compensate for electrode displacement due to brain shift (Step 23). Moreover, FreeSurfer automatically registers the subject's brain to a template brain on the basis of its cortical gyrification pattern, an aspect of brain structure that remains difficult to accurately normalize using volume-based registration techniques due to its complexity and variability across subjects[38,39]. Our protocol uses the resulting surface-registration maps to link surface electrode positions to their template homologs, preserving the spatial relationship between cortical folds and electrodes in each subject (Step 30). This makes the surface-based registration technique particularly effective for generalizing across subjects, facilitating more accurate group-level analysis based on individual peak activity sites or cortically interpolated activity (i.e., projecting and averaging activity from multiple subjects on a cortical mesh of FreeSurfer's 'fsaverage' template brain instead of the subject's brain as in Step 51). Finally, FreeSurfer-generated atlases are convenient for representations of neural and anatomical data for a single subject (Step 53), as they are defined in native subject space. Other supported atlases are defined in standardized (e.g., Montreal Neurological Institute (MNI)) space and require the added step of transforming electrode positions to that space.

Specific considerations when processing human intracranial data

Anatomical images, typically MRI and CT scans, are used as part of the epilepsy diagnostic and surgical procedures. A pre-implant MRI shows the anatomy of the head, including the brain, and is used to identify structural abnormalities. An MRI is also instrumental in guiding SEEG electrode implantation subsequent to the clinical decision to record intracranially. A post-implant CT shows high-intensity objects such as the electrodes and skull but lacks details of brain anatomy. To obtain knowledge of an electrode's location in relation to the brain's anatomy, the two scans must be fused.

After fusion of the pre- and postoperative anatomical images, electrodes that have been surgically placed on the cortical surface occasionally appear 'buried' within the cortical tissue, sometimes more than a centimeter deep[40–45]. This electrode displacement is typically due to 'brain shift', the inward sinking of the brain post implant that is most commonly observed with electrocorticographic surface grid electrodes. The brain shift reflects tissue displacement caused by the electrodes themselves and by subdural fluid loss or accumulation. As noted, the displacement is most pronounced directly below a craniotomy and is usually minimal for implants solely involving burr holes[45]. It is important to account for this brain shift in order to accurately align electrode-specific signals with the local cortical anatomy. Several labs have developed re-alignment techniques to compensate for electrode displacement due to brain shift, reducing localization error to <3 mm as compared with that of intraoperative photographs[11,25–32]. Our protocol currently supports two of these techniques to project electrode grids back to the cortical surface. One method that we demonstrate in Step 23 involves an optimization algorithm that minimizes an energy function defined by inter-electrode distances and global deformation of the electrode configuration[32]. The other method projects electrodes to the surface of the brain in the direction of the local norm vector of the electrode grid[25].

Electrode localization can also be performed using post-implant MRIs, although these are not commonly acquired in a clinical setting. These scans show the brain anatomy after electrode implantation, so brain shift is not an issue. In a T1-weighted MRI, electrodes appear dark, owing to the magnetic susceptibility artifact. This is generally not an issue for recordings with depth electrodes (SEEG), in which the electrodes are visible as dark voids in the higher-intensity brain tissue. Electrode grids and strips (ECoG), on the other hand, are placed directly on the cortical surface. This complicates their identification, as the electrodes are surrounded by cerebral spinal fluid, which also appears dark on a T1 scan (but see refs [27,46–48] for workarounds). In the rare case that a post-implant MRI is available that is of sufficient quality to clearly show the electrodes, the CT preprocessing and fusion steps (Steps 9–15) may be left out. In this situation, the electrode localization may be
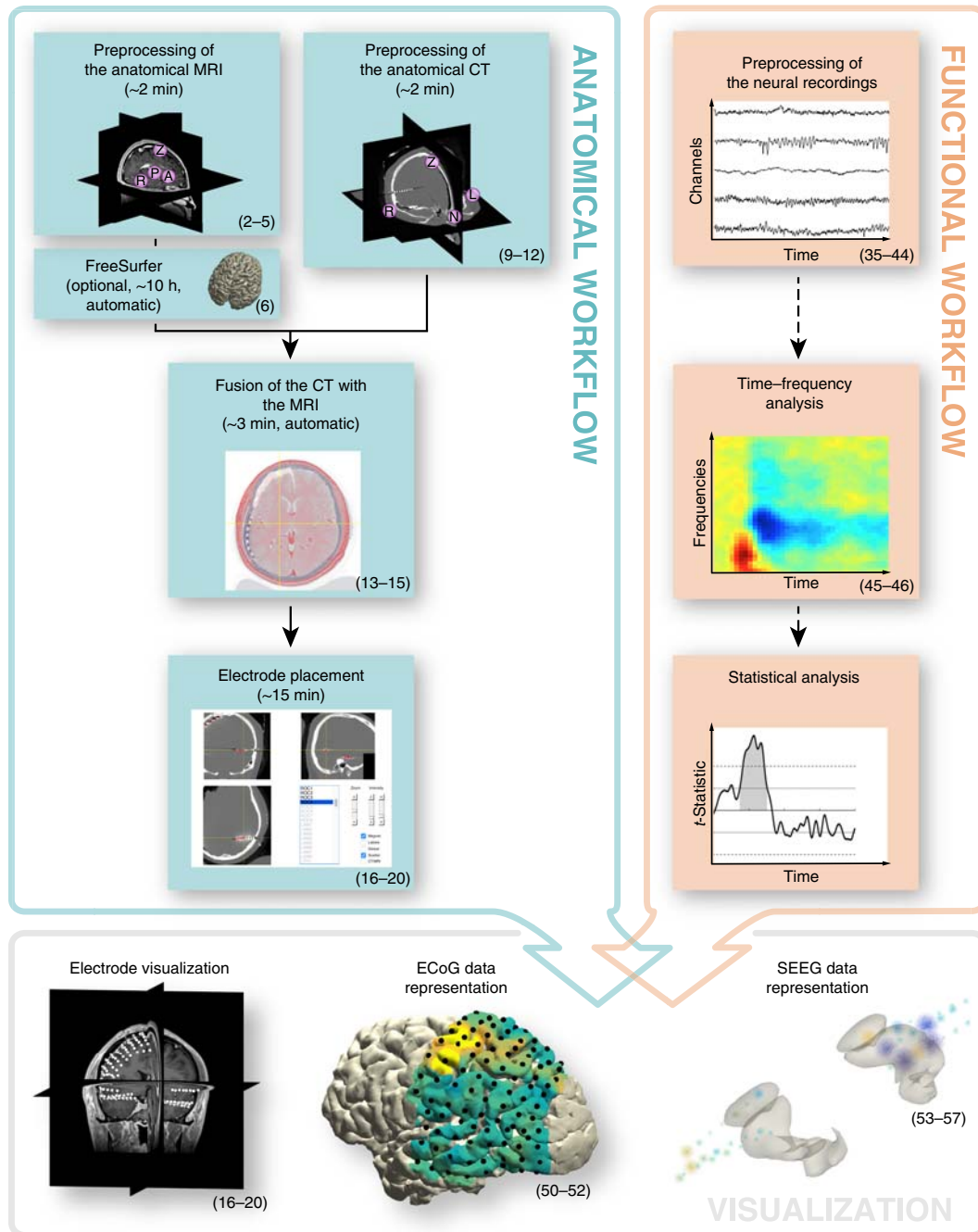
Fig. 1 | Overview of the procedure. The protocol comprises two parallel but interrelated workflows. The anatomical workflow minimally consists of the preprocessing and fusion of the anatomical images and electrode placement. The functional workflow encompasses the preprocessing of the neural recordings but may also include follow-up activities, such as event-related averaging, time–frequency analysis, and statistical analysis. The electrode-placement activity offers the opportunity to directly link anatomical locations to electrode labels corresponding to the neural recordings, allowing for an early seamless integration of the two workflows to facilitate anatomically informed data exploration and visualization. The numbers in parentheses indicate the step numbers of the procedure in which the activities are described.

performed on the post-implant MRI. Furthermore, in the case of single-unit recordings, a post-implant MRI may be required to localize the microwires. However, if the post-implant MRI is of unsatisfactory quality in regard to brain anatomy, for instance, due to electrode-induced MR signal distortion, we recommend fusing the post-implant MRI with the pre-implant MRI, as if it were a post-implant CT.

Neural recordings are typically part of the ongoing clinical monitoring and come in various file formats. Each data channel represents, as a function of time, the electric potential difference, obtained

with either a bipolar or referential electrode scheme. Thus, the electrodes are pairwise linked or referenced to a single, common electrode during acquisition. The latter montage has the benefit that the recordings can be easily remontaged to a more preferred scheme in the off-line analysis[49]. The markers or triggers for stimulus-onset times and responses are typically recorded simultaneously in a dedicated channel, allowing for precise synchronization of experimental scenarios with the neural recording.

Overview of the procedure

The protocol has two parallel but interrelated workflows, as shown in Fig. 1. Anatomical data are processed in the first workflow. The main components of the first workflow are the preprocessing and fusion of the anatomical images, and electrode placement (Steps 1–20). Secondary activities that might be required include cortical surface extraction with FreeSurfer (Step 6), and brain-shift compensation, spatial normalization, and anatomical labeling (Steps 21–34). Generally, the anatomical workflow aims to obtain estimates of the electrode locations in relation to the individual and atlas-based brain anatomy, which is a one-time procedure for each subject. The second workflow improves the signal-to-noise ratio and extracts the relevant features from the electrophysiological data while preparing for subsequent analyses. The minimal component is the preprocessing of the neural recordings (Steps 35–44), but this part of the protocol can also include follow-up activities such as time–frequency (Steps 45 and 46) and single-subject or group-level statistical analysis (not covered in the procedure). Generally, the specifics of the functional workflow depend ultimately on the clinical or research question at hand and contingencies in the experimental paradigm.

The two workflows become connected for the first time during the electrode-placement activity (Step 17), which offers the opportunity to directly link anatomical locations to electrode labels corresponding to the neural recordings. Electrode placement involves a graphical user interface designed for efficient yet precise identification of electrodes in even the most challenging cases. The integration of the two workflows culminates in an interactive and anatomically informed data-exploration tool and the ability to represent functional and epileptiform neural activity overlaid on cortical and subcortical surface models, in figure or video format (Steps 47–57).

Implementation and adaptation of the procedure

All parts of the procedure, except for FreeSurfer, run on a single universal platform (MATLAB), which enables relatively easily automated procedures that can deal with repeated analyses within and across subjects. We recommend that the user construct a single script for a single subject by copying and pasting code from this protocol into the MATLAB editor (e.g., Supplementary Data 1), and evaluating segments of that script in the MATLAB command window. Once the script produces satisfactory results, it can be converted into a batch analysis by breaking it into separate components. By looping around the separate components for all subjects, the entire analysis pipeline for all subjects in a study can easily be executed and intermediate results can be saved and evaluated.

The whole batch can be documented and shared, or re-evaluated with different parameter settings, as appropriate. Because single parameters can be changed at a function call, alternation between various fusion, localization, projection, normalization, filtering, remontaging, and spectral estimation algorithms can be achieved, accommodating analysis of different cases and situations. The output data structures are kept consistent across the different algorithms, and the parameters of the used algorithm are appended to allow for access to the full data provenance at any level of the analysis pipeline (Box 1).

Datasets that can be processed

Example dataset

In the procedure, we explain each part of the data processing but also provide specific instructions that enable analysis of an example iEEG dataset. Further information about this dataset is provided in the Materials section.

We chose this iEEG dataset as an illustrative example for three reasons. First, it contains neural recordings from both cortical grid (ECoG) and stereotactically inserted depth electrodes (SEEG), requiring strategies for dealing with each type, as well as their combination, in the analysis. Second, the pre-implant MRI is not of the best quality (a contrast agent was used), electrodes of adjacent cortical grids have seemingly merged with one another in the post-implant CT, and there is substantial electrode displacement owing to a subdural hygroma contributing to brain shift. These issues are common in intracranial data analysis and, hence, it is important that users understand how to deal

with nonideal data. By processing this example dataset, users must undertake all the fundamental steps required to analyze intracranial data, and these steps are independent of the experimental paradigm being investigated[20,24,50]. This example demonstrates the analysis of task-related high-frequency-band activity (~70–150 Hz), a prominent neural signature in intracranial data that has been associated with neuron population-level firing rate[5,51–54]. Many other examples of analyses that can be undertaken, such as event-related potential analysis, connectivity analysis, and statistical analysis, have been described in detail elsewhere[55–57].

Supported data formats

The following anatomical data formats can be analyzed using this protocol:

- AFNI (*.head, *.brik)
- Analyze (*.img, *.hdr)
- ANT (*.mri)
- BioImage Suite (*.mgrid)
- DICOM (*.dcm, *.ima)
- FreeSurfer (*.mgz, *.mgh)
- MINC (*.mnc)
- NIfTI (*.nii, *.nii.gz)

    The following electrophysiological data formats can be analyzed using this protocol:

- Anywave (*.ah5)
- BCI2000 (*.dat)
- BESA (*.besa)
- Blackrock (*.nev, *.ns#)
- Cambridge Electronic Design (*.smr)
- European Data Format (*.edf)
- GTec (*.mat, *.hdf5)
- Micromed (*.trc)
- Neuralynx (*.ncs, *.nse, *.nts, *.nst, *.ntt, *.nev)
- Neuromag (*.fif)
- Neuroscope (*.eeg, *.dat, *.xml)
- Nihon Kohden (*.m00, *.eeg)
- Plexon (*.ddt, *.nex, *.plx)
- Various EEG, MEG, NIRS, and eye-tracker data formats

Materials

Equipment

Data

- Suitable datasets that can be used are discussed in the Introduction, and details of the example dataset are given in Box 2. **! CAUTION** The acquisition and subsequent analysis of data from human subjects must conform to institutional and national regulations. Informed consent must be obtained from experimental subjects for all procedures being undertaken.

Software

- MATLAB environment (MathWorks; installation and licensing through http://www.mathworks.com)
- FieldTrip toolbox (Box 1; freely available at http://www.fieldtriptoolbox.org, code: https://github.com/fieldtrip/fieldtrip)
- FreeSurfer software suite for cortical surface extraction (optional; freely available at http://www.freesurfer.net)

Procedure

Specification of subject ID ● Timing ~1 min

1 Specify the subject ID using the below command.

```
subjID = 'SubjectUCI29'
```

    This ID will be used in the file naming, in addition to information about the type of data (e.g., MRI, CT), the coordinate system that is used (e.g., ACPC, MNI), and the

process(es) that were applied to it (e.g., 'f' for fusion). For example, a CT scan that is aligned to the ACPC (Anterior Commissure - Posterior Commissure) coordinate system and that has just been fused with the anatomical MRI is written out to a file as subjID_CT_acpc_f.nii.

Box 2 | Example dataset

We describe specifically how to process an example dataset acquired at the Medical Center of the University of California, Irvine. The Office for the Protection of Human Subjects of the University of California, Berkeley, approved the study, and the subject gave informed consent. The components of the dataset are listed below. The dataset contains three anatomical images plus neural recordings from 96 ECoG and 56 SEEG electrodes that were implanted as part of preparation for epilepsy surgery. The neural data were recorded in the context of an experiment that required the patient to press a button with the right hand when hearing a target tone. All neural recordings were acquired using a Nihon Kohden recording system with a JE-120A amplifier, analog-filtered above 0.01 Hz and digitally sampled at 5 kHz. The sequence imaging parameters used for the MRI were MP-RAGE, 256 × 256 × 176 mm with 1 × 1 × 1-mm isotropic voxels. The original dataset (after defacing the imaging data with `ft_defacevolume`) and the processed results are available for download from the online repository at https://doi.org/10.5281/zenodo.1201560. Raw DICOM images and recording files are not shared, in order to protect the subject's identity.

Anatomical images
- Pre-implant T1-weighted MRI, SubjectUCI29_MR_acpc.nii (MRI, Siemens 3T TrioTim)
- Post-implant CT, SubjectUCI29_CT_acpc_f.nii (CT, Philips iCT 256)
- Post-implant T1-weighted MRI, SubjectUCI29_postimpl_MR_acpc_f.nii (MRI, Siemens 1.5T Avanto). This scan is not used in the Procedure but is nevertheless included for completeness.

Neural recordings
- The preprocessed neural recordings are in SubjectUCI29_data.mat.
- 64-Contact cortical grid with left parietal coverage (Integra, 8×8 layout, 10-mm inter-electrode spacing, labels have an 'LPG' prefix)
- 32-Contact cortical grid with left temporal coverage (Integra, 4×8 layout, 10-mm inter-electrode spacing, labels have an 'LTG' prefix)
- Eight-contact linear depth electrode targeting the left amygdala (Ad-Tech, 5-mm inter-electrode spacing, labels have a 'LAM' prefix)
- Eight-contact linear depth electrode targeting the left hippocampus head (Ad-Tech, 5-mm inter-electrode spacing, labels have an 'LHH' prefix)
- Eight-contact linear depth electrode targeting left hippocampus tail (Ad-Tech, 5-mm inter-electrode spacing, labels have an 'LTH' prefix)
- Eight-contact linear depth electrode targeting the right amygdala (Ad-Tech, 5-mm inter-electrode spacing, labels have a 'RAM' prefix)
- Eight-contact linear depth electrode targeting the right hippocampus head (Ad-Tech, 5-mm inter-electrode spacing, labels have an 'RHH' prefix)
- Eight-contact linear depth electrode targeting the right hippocampus tail (Ad-Tech, 5-mm inter-electrode spacing, labels have an 'RTH' prefix)
- Eight-contact linear depth electrode targeting the right occipital cortex (Ad-Tech, 5-mm inter-electrode spacing, labels have a 'ROC' prefix)

Box 3 | Coordinate system determination ● **Timing** ~1 min

Coordinate systems define the orientation and units of the *x*, *y*, and *z* axes of an anatomical volume, in addition to an origin point along the brain's midline (e.g., AC). Here, we provide a guideline for determining the native coordinate system of the MRI and CT scans and, in particular, whether they have a left-to-right or a right-to-left orientation. Knowledge of the orientation of the left–right axis of the scan's native coordinate system provides the necessary context for demarcating the right-hemisphere landmark in the succeeding alignment step. Although the interpretation of posterior–anterior and inferior–superior axes is straightforward from axial, coronal, or sagittal slices of the brain, differentiating left from right requires a 3D context. To accomplish this, we recommend using `ft_determine_coordsys`, which depicts an anatomical volume as three intersecting, orthogonal slices and labels the *x*, *y*, and *z* axes. This allows the axis that represents the left–right axis to be identified and, importantly, determines whether that axis has a left-to-right or a right-to-left orientation (see Supplementary Video 1 for further guidance).

1 Visualize the coordinate system of the MRI or CT by inputting the following command:
   `ft_determine_coordsys(mri)`
2 Determine which of the three axes, *x*, *y*, or *z*, runs through or along the left–right axis of the subject's head. This axis is the left–right axis for this anatomical volume.
3 Determine the orientation of the left–right axis. If the values on the left–right axis increase to the right (indicated by a '+' sign), then the scan has a left-to-right orientation. If the values on the left–right axis increase to the left, then the scan has a right-to-left orientation.
4 Write down the orientation of the scan's left–right axis.

Preprocessing of the anatomical MRI ● Timing ~2 min

2 Import the anatomical MRI (for the example dataset, this is the file named SubjectUCI29_MR_acpc.nii) into the MATLAB workspace using `ft_read_mri` with the below command.

```
mri = ft_read_mri(<path to MRI file>);
```

   The MRI comes in the format of a single file with an .img or .nii extension, or a folder containing a series of files with a .dcm or .ima extension (The code in Supplementary Data 2 may aid in the search and visualization of these DICOM series.).

3 Determine the native orientation of the anatomical MRI's left–right axis using `ft_determine_coordsys` as described in Box 3 and Supplementary Video 1.

4 Using the below command, align the anatomical MRI to the ACPC coordinate system[58], a preferred convention for the FreeSurfer operation optionally used at Step 6. In this coordinate system, the origin (coordinate [0,0,0]) is at the anterior commissure (AC), the y axis runs along the line between the AC and the posterior commissure (PC), and the z axis lies in the midline dividing the two cerebral hemispheres. Specify the AC and PC, an interhemispheric location along the midline at the top of the brain, and a location in the brain's right hemisphere. If the scan was found to have a left-to-right orientation in the previous step, the right hemisphere is identified as the hemisphere having larger values along the left–right axis. Vice versa, in a right-to-left system, the right hemisphere has smaller values along that axis than does its left counterpart (see Supplementary Video 2 for further guidance).

```
cfg = [];
cfg.method = 'interactive';
cfg.coordsys = 'acpc';
mri_acpc = ft_volumerealign(cfg, mri);
```

   ▲ **CRITICAL STEP** To correctly fuse the MRI and CT scans at a later step, accuracy in demarcating the right-hemisphere landmark is important for avoiding an otherwise hard-to-detect flip of the scan's left and right orientation.

5 Write the preprocessed anatomical MRI out to a file as shown below.

```
cfg = [];
cfg.filename = [subjID '_MR_acpc'];
cfg.filetype = 'nifti';
cfg.parameter = 'anatomy';
ft_volumewrite(cfg, mri_acpc);
```

(Optional) Cortical surface extraction with FreeSurfer ● Timing ~10 h, automatic

▲ **CRITICAL** Although optional, processing of the anatomical MRI with FreeSurfer can be beneficial for subsequent analysis and data interpretation, as discussed in the Introduction.

6 Execute FreeSurfer's `recon-all` functionality from the Linux or MacOS terminal (Windows via VirtualBox), or from the MATLAB command window as detailed below.

```
fshome = <path to freesurfer home directory>;
subdir = <path to subject directory>;
mrfile = <path to subject MR_acpc.nii>;
system(['export FREESURFER_HOME=' fshome '; ' ...
'source $FREESURFER_HOME/SetUpFreeSurfer.sh; ' ...
'mri_convert -c -oc 0 0 0 ' mrfile ' ' [subdir '/tmp.nii'] '; ' ...
'recon-all -i ' [subdir '/tmp.nii'] ' -s ' 'freesurfer' ' -sd ' subdir '
-all'])
```

   This set of commands will create a folder named 'freesurfer' in the subject directory, with subdirectories containing a multitude of FreeSurfer-generated files.

   ■ **PAUSE POINT** FreeSurfer's fully automated segmentation and cortical extraction of the anatomical MRI can take 10 h or more, so the program can be left to run overnight. To avoid delay when working through the example dataset, the online repository containing the example dataset also contains the output from FreeSurfer that is obtained from this step in a folder named 'freesurfer'.

7 Import the extracted cortical surfaces into the MATLAB workspace and examine their quality.

```
pial_lh = ft_read_headshape(<path to freesurfer/surf/lh.pial>);
pial_lh.coordsys = 'acpc';
ft_plot_mesh(pial_lh);
lighting gouraud;
```

```
camlight;
```
Repeat the above code using `rh.pial` to visualize the pial surface of the right hemisphere.

? TROUBLESHOOTING

8   Import the FreeSurfer-processed MRI (from Step 6) into the MATLAB workspace for the purpose of fusing with the CT scan at Step 13, and specify the coordinate system to which it was aligned in Step 4, using the following command:
```
fsmri_acpc = ft_read_mri(<path to freesurfer/mri/T1.mgz>);
fsmri_acpc.coordsys = 'acpc';
```

Preprocessing of the anatomical CT ● Timing ~2 min

9   Import the anatomical CT (for the example dataset, this is the file named 'SubjectUCI29_CT_acpc_f.nii') into the MATLAB workspace using the below command.
```
ct = ft_read_mri(<path to CT file>);
```
Similar to the MRI, the CT scan comes in the format of a single file with an .img or .nii extension, or a folder containing a series of files with a .dcm or .ima extension. (The code in Supplementary Data 2 can be used to search and visualize a DICOM series.)

10 If the laterality of the electrode implantation is not known, determine the native orientation of the anatomical CT's left–right axis using `ft_determine_coordsys` and following the steps given in Box 3 and Supplementary Video 1.

11 Align the anatomical CT to the CTF head surface coordinate system by specifying the nasion (at the root of the nose), left and right pre-auricular points (just in front of the ear canals), and an interhemispheric location along the midline at the top of the brain using the following command (this step is also shown in Supplementary Video 3):
```
cfg = [];
cfg.method = 'interactive';
cfg.coordsys = 'ctf';
ct_ctf = ft_volumerealign(cfg, ct);
```
The CT scan is initially aligned to the CTF head surface coordinate system because the ACPC coordinate system used for the MRI relies on neuroanatomical landmarks that are not visible in the CT.

▲ **CRITICAL STEP** To correctly fuse the MRI and CT scans at Step 13, accuracy in demarcating the right and left pre-auricular landmark in this step is important for avoiding an otherwise hard-to-detect flip of the scan's left and right orientation.

12 Automatically convert the CT's coordinate system into an approximation of the ACPC coordinate system, the same system to which the anatomical MRI was aligned, using the below command.
```
ct_acpc = ft_convert_coordsys(ct_ctf, 'acpc');
```

Fusion of the CT with the MRI ● Timing ~3 min

13 Fuse the CT with the MRI using the below command.
```
cfg = [];
cfg.method = 'spm';
cfg.spmversion = 'spm12';
cfg.coordsys = 'acpc';
cfg.viewresult = 'yes';
ct_acpc_f = ft_volumerealign(cfg, ct_acpc, fsmri_acpc);
```
Fusion of the scans is necessary to link the electrode locations in the anatomical CT to their corresponding locations in the anatomical MRI[59,60]. Given that both scans are from the same subject and their common denominator is the skull, a rigid-body transformation suffices for their alignment under normal circumstances (the default technique when using the SPM method in FieldTrip).

14 Carefully examine the interactive figure that is produced after the co-registration is completed, showing the MRI and fused CT superimposed. A successful fusion will show tight interlocking of CT-positive skull (in blue) and MRI-positive brain and skin tissue (in red).

▲ **CRITICAL STEP** Accuracy of the fusion operation is important for obtaining precise knowledge of the location of the electrode and the part of the brain from which the local electrophysiological signal has originated. It is also important for correctly placing the electrodes in an anatomical context at Step 33.

? TROUBLESHOOTING
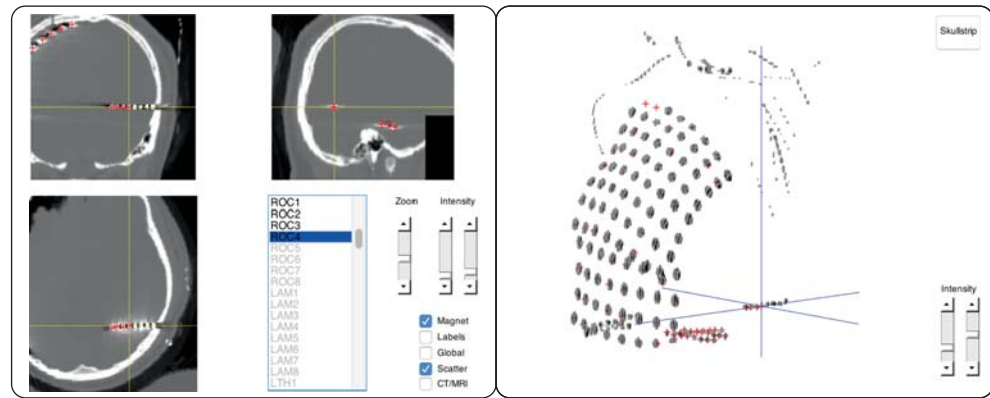
Fig. 2 | Interactive electrode placement. Clicking an electrode label in the main panel on the left will directly assign that label to the current crosshair position in the CT scan. Several features facilitate precise navigation of the anatomical CT, such as a zoom mode, a magnet option that transports the crosshair to the nearest weighted maximum (or minimum in the case of a post-implant MRI), and the interactive 3D scatter figure shown on the right.

15 Write the MRI-fused anatomical CT out to a file using the command below.
```
cfg = [];
cfg.filename = [subjID '_CT_acpc_f'];
cfg.filetype = 'nifti';
cfg.parameter = 'anatomy';
ft_volumewrite(cfg, ct_acpc_f);
```

Electrode placement ● Timing ~15 min

16 Import the header information from the recording file, if possible, using the command below.
```
hdr = ft_read_header(<path to recording file>);
```
By giving the electrode labels originating from the header as input to `ft_electrodeplacement` in the next step, the labels will appear as a to-do list during the interactive electrode-placement activity. A second benefit to this step is that the electrode locations can be directly assigned to labels collected from the recording file, obviating the need to sort and rename electrodes to match the electrophysiological data.

17 Localize the electrodes in the post-implant CT with `ft_electrodeplacement`, as shown in Fig. 2. Clicking an electrode label in the list will directly assign that label to the current crosshair location (also demonstrated in Supplementary Video 4). Several in-app features facilitate efficient yet precise navigation of the anatomical image, such as a zoom mode, a magnet option that transports the crosshair to the nearest weighted maximum with subvoxel accuracy (or minimum in the case of a post-implant MRI), and an interactive 3D scatter figure that is linked to the 2D volume representations. Use the command below to pass on the pre-implant MRI, `fsmri_acpc`, to `ft_electrodeplacement` to allow toggling between the CT and MRI views for the identification of specific electrodes based on their anatomical location. Generally, electrode 1 is the electrode farthest away from the craniotomy or burr hole in the case of depths and single-row strips. To determine the numbering of grid and multirow strip electrodes, it is important that careful notes be taken during surgery and recording.
```
cfg = [];
cfg.channel = hdr.label;
elec_acpc_f = ft_electrodeplacement(cfg, ct_acpc_f, fsmri_acpc);
```

? TROUBLESHOOTING

18 Examine whether the variables in the resulting electrode structure `elec_acpc_f` match the recording parameters, e.g., the number of channels stored in the `label` field, by typing `elec_acpc_f` into the command window.
```
elec_acpc_f =
unit: 'mm'
coordsys: 'acpc'
label: {152x1 cell}
```

```
elecpos: [152x3 double]
chanpos: [152x3 double]
tra: [152x152 double]
cfg: [1x1 struct]
```

The electrode and channel positions are stored in the *elecpos* and *chanpos* fields, respectively. The *elecpos* field contains the original electrode positions. With the exception of possible brain-shift compensation, this field is not adjusted. The channel positions in the *chanpos* field are initially identical to the electrode positions but may be updated to accommodate off-line adjustments in channel combinations, i.e., during remontaging. For bipolar iEEG data, the channel position considered the best is between the two corresponding electrode positions. The *chanpos* field is used for overlaying the neural data on (sub-)cortical models during data visualization. The *tra* field is a matrix with the weight of each electrode into each channel, which at this stage merely is an identity matrix reflecting one-to-one mappings between electrodes and channels.

19 Using the command below, visualize the MRI along with the electrodes and their labels and examine whether they show the expected behavior.

```
ft_plot_ortho(fsmri_acpc.anatomy, 'transform', fsmri_acpc.transform,
'style', 'intersect');
ft_plot_sens(elec_acpc_f, 'label', 'on', 'fontcolor', 'w');
```

? TROUBLESHOOTING

20 Using the command below, save the resulting electrode information to a file.

```
save([subjID '_elec_acpc_f.mat'], 'elec_acpc_f');
```

Brain-shift compensation (optional for cortical grids and strips) ● Timing ~5 min

21 In the case of 'brain shift', i.e., the inward displacement of brain tissue and electrodes due to pressure changes related to the craniotomy, re-alignment of electrode grids to the pre-implant cortical surface may be necessary. To prevent inwardly displaced electrodes from being incorrectly placed in nearby cortical sulci during back-projection, create a smooth hull around the cortical mesh generated by FreeSurfer[61] using the command below. This hull tracks the (exposed) outer surface on which the cortical grid rested.

```
cfg = [];
cfg.method = 'cortexhull';
cfg.headshape = <path to freesurfer/surf/lh.pial>;
cfg.fshome = <path to freesurfer home directory>;
hull_lh = ft_prepare_mesh(cfg);
```

22 Save the hull to a file using the command below.

```
save([subjID '_hull_lh.mat'], hull_lh);
```

23 Using the command below, project the electrode grids to the surface hull of the implanted hemisphere. Given that different grids can move independently from one another and that the projection algorithm specified in `cfg.warp` considers the global electrode configuration of a grid[32], it is recommended to re-align electrode grids individually by running separate re-alignment procedures for each grid. Here, we re-align the electrodes of the left parietal grid, followed by alignment of the electrodes of the left temporal grid (LPG and LTG, respectively) and store the updated grid electrode information in a new variable together with the unaltered coordinates of the depth electrodes.

```
elec_acpc_fr = elec_acpc_f;
grids = {'LPG*', 'LTG*'};
for g = 1:numel(grids)
cfg = [];
cfg.channel = grids{g};
cfg.keepchannel = 'yes';
cfg.elec = elec_acpc_fr;
cfg.method = 'headshape';
cfg.headshape = hull_lh;
cfg.warp = 'dykstra2012';
cfg.feedback = 'yes';
elec_acpc_fr = ft_electroderealign(cfg);
end
```
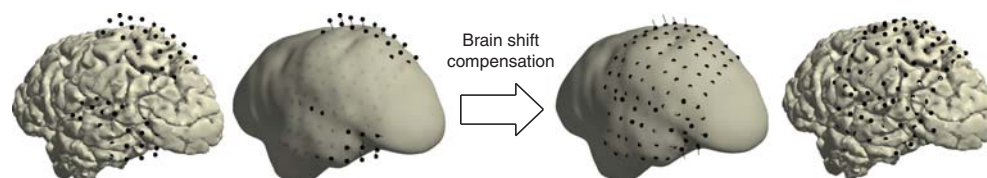
Fig. 3 | Brain-shift compensation. In some patients, compensation for electrode displacement due to brain shift after implantation may be necessary. In this particular case, a subdural hygroma at the top of the brain caused severe electrode displacement in a direction opposite to the more commonly observed inward shift (left). Re-aligning electrode grids to the cortical surface can compensate for electrode displacement due to brain shift (right). The thin black lines indicate each electrode's path from its localized origin on the left to its projected location on the right.

24 Using the command below, visualize the cortex and electrodes together and examine whether they show the expected behavior (Fig. 3).

```
ft_plot_mesh(pial_lh);
ft_plot_sens(elec_acpc_fr);
view([-55 10]);
material dull;
lighting gouraud;
camlight;
```

▲ **CRITICAL STEP** Accuracy of the re-alignment operation is important for obtaining precise knowledge of the location of the electrode and the part of the brain from which the local electrophysiological signal has originated. It is also important for correctly placing the electrodes in an anatomical context at Step 33.

? troubleshooting

25 Using the command below, save the updated electrode information to a file.

```
save([subjID '_elec_acpc_fr.mat'], 'elec_acpc_fr');
```

**(Optional) Volume-based registration** ● **Timing** ~2 min

▲ **CRITICAL** FieldTrip supports looking up the anatomical or functional labels corresponding to the electrodes in a number of atlases, including the AFNI Talairach–Tournoux atlas[62], the AAL atlas[63], the BrainWeb dataset[64], the JuBrain Cytoarchitectonic Atlas[65], the VTPM atlas[66], and the Brainnetome Atlas[67], in addition to the subject-tailored Desikan–Killiany and Destrieux atlases produced by FreeSurfer[68,69]. Given that no two electrodes end up in exactly the same location across subjects because of inter-individual variability in electrode coverage and brain anatomy, atlases are particularly useful for the systematic combination of neural activity from different subjects in a so-called ROI analysis. With the exception of the FreeSurfer-based atlases (Desikan–Killiany and Destrieux), the atlases are in MNI coordinate space. If using an atlas in MNI coordinate space, spatially normalize the electrodes by following Steps 26 and 27.

26 To generalize the electrode coordinates to other brains or MNI-based neuroanatomical atlases at Step 33, register the subject's brain to the standard MNI brain using the command below. The volume-based registration technique considers the overall geometry of the brain[70] and can be used for the spatial normalization of all types of electrodes, whether at depth or on the surface.

```
cfg = [];
cfg.nonlinear = 'yes';
cfg.spmversion = 'spm12';
fsmri_mni = ft_volumenormalise(cfg, fsmri_acpc);
```

27 Use the resulting deformation parameters to obtain the electrode positions in standard MNI space with the command below.

```
elec_mni_frv = elec_acpc_fr;
elec_mni_frv.elecpos  =  ft_warp_apply(fsmri_mni.params,  ele-
c_acpc_fr.elecpos, 'individual2sn');
elec_mni_frv.chanpos  =  ft_warp_apply(fsmri_mni.params,  ele-
c_acpc_fr.chanpos, 'individual2sn');
elec_mni_frv.coordsys = 'mni';
```
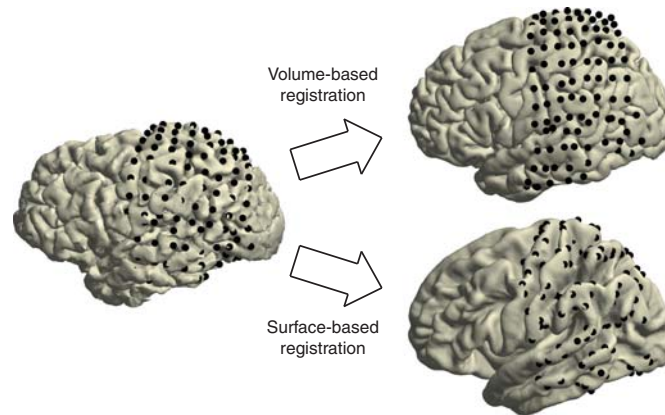
Fig. 4 | Spatial normalization. On the left are the electrodes on the individual cortical sheet. The top right shows the electrodes on the standard MNI brain after volume-based registration. The bottom right shows the electrodes on FreeSurfer's fsaverage brain after surface-based registration. Compared with volume-based registration, with surface-based registration, the original grid geometry is no longer preserved as electrodes are moved from one brain to another according to the curvature pattern of the cortex.

28 Using the command below, visualize the cortical mesh extracted from the standard MNI brain along with the spatially normalized electrodes and examine whether they show the expected behavior given the electrodes' original anatomical locations (top right in Fig. 4).

▲ **CRITICAL STEP** Accuracy of the volume-based registration is important for group-level analysis of brain activity and for correctly overlaying the electrode positions with a brain atlas at Step 33.

```
load(<path to fieldtrip/template/anatomy/surface_pial_left.mat>);
ft_plot_mesh(mesh);
ft_plot_sens(elec_mni_frv);
view([-90 20]);
material dull;
lighting gouraud;
camlight;
```

? TROUBLESHOOTING

29 Using the command below, save the normalized electrode information to a file.

```
save([subjID '_elec_mni_frv.mat'], 'elec_mni_frv');
```

Surface-based registration (optional for surface electrodes) ● Timing ~2 min

30 To enable the generalization of the electrode coordinates to other brains using the surface-based registration technique, map the electrodes onto FreeSurfer's fsaverage brain with the command below. The surface-based registration technique considers only the curvature patterns of the cortex[37] and thus can be used for the spatial normalization of electrodes located on or near the cortical surface. In the example case, this pertains to all electrodes of the left parietal and temporal grids.

```
cfg = [];
cfg.channel = {'LPG*', 'LTG*'};
cfg.elec = elec_acpc_fr;
cfg.method = 'headshape';
cfg.headshape = <path to freesurfer/surf/lh.pial>;
cfg.warp = 'fsaverage';
cfg.fshome = <path to freesurfer home directory>;
elec_fsavg_frs = ft_electroderealign(cfg);
```

31 Using the command below, visualize FreeSurfer's fsaverage brain, along with the spatially normalized electrodes, and examine whether they show the expected behavior (bottom right in Fig. 4).

▲ **CRITICAL STEP** Accuracy of the surface-based registration is important for group-level analysis of cortical activity.

```
fspial_lh = ft_read_headshape(<path to fshome/subjects/fsaverage/
surf/lh.pial>);
fspial_lh.coordsys = 'fsaverage';
```

```
ft_plot_mesh(fspial_lh);
ft_plot_sens(elec_fsavg_frs);
view([-90 20]);
material dull;
lighting gouraud;
camlight;
```

32 Using the command below, save the normalized electrode information to a file.
```
save([subjID '_elec_fsavg_frs.mat'], 'elec_fsavg_frs');
```

(Optional) Anatomical labeling ● Timing ~1 min

33 Import the brain atlas of interest, e.g., the AAL atlas, into the MATLAB workspace using the below command.
```
atlas = ft_read_atlas(<path to fieldtrip/template/atlas/aal/ROI_M-
NI_V4.nii>);
```

34 Using the command below, look up the corresponding anatomical label of an electrode of interest, e.g., electrode LHH1, targeting the left hemisphere's hippocampus.
```
cfg = [];
cfg.roi = elec_mni_frv.chanpos(match_str(elec_mni_frv.label, 'LHH1'),:);
cfg.atlas = atlas;
cfg.inputcoord = 'mni';
cfg.output = 'label';
labels = ft_volumelookup(cfg, atlas);
[~, indx] = max(labels.count);
labels.name(indx)
ans =
   'ParaHippocampal_L'
```
Supplementary Data 3 is a tool that automatically overlays all channels in an electrode structure with all of the atlases listed above and stores the resulting anatomical labels in an Excel table (e.g., SubjectUCI29_electable.xlsx in the online repository).

? TROUBLESHOOTING

Preprocessing of the neural recordings ● Timing ~10 min

35 Using the command below, define the trials, that is, the segments of data that will be used for further processing and analysis. This step produces a matrix, *cfg.trl*, containing for each segment the begin and end sample in the recording file. In the case of the example provided in the shared data, the segments of interest begin 400 ms before tone onset, are marked with a '4' in the trigger channel, and end 900 ms thereafter.
```
cfg = [];
cfg.dataset = <path to recording file>;
cfg.trialdef.eventtype = 'TRIGGER';
cfg.trialdef.eventvalue = 4;
cfg.trialdef.prestim = 0.4;
cfg.trialdef.poststim = 0.9;
cfg = ft definetrial(cfg);
```

36 Using the command below, import the data segments of interest into the MATLAB workspace and filter the data for high-frequency and power-line noise (type `help ft_preprocessing` for filtering options).
```
cfg.demean = 'yes';
cfg.baselinewindow = 'all';
cfg.lpfilter = 'yes';
cfg.lpfreq = 200;
cfg.padding = 2;
cfg.padtype = 'data';
cfg.bsfilter = 'yes';
cfg.bsfiltord = 3;
cfg.bsfreq = [59 61; 119 121; 179 181];
data = ft_preprocessing(cfg);
```

37 Examine whether the variables in the output data structure match the recording and preprocessing parameters, i.e., the sampling rate (fsample), number of recording channels (label), and segmentation into the experiment's 26 trials (trial, and their respective time axes in time) by typing data in the command window.

```
data =
label: {152x1 cell}
time: {1x26 cell}
trial: {1x26 cell}
fsample: 5000
sampleinfo: [26x2 double]
cfg: [1x1 struct]
```

38 Using the command below, add the *elec* structure originating from the anatomical workflow and save the preprocessed electrophysiological data to a file.

```
data.elec = elec_acpc_fr;
save([subjID '_data.mat'], 'data');
```

The advantage of adding the electrode information at this stage is that it will be kept consistent with the neural data going forward, as when applying the same montage used for the neural recordings to the channel positions.

39 Inspect the neural recordings using ft_databrowser with the command below and identify channels or segments of noninterest, for instance, segments containing signal artifacts or (in this case) epileptiform activity. Mark the poor-quality segments by drawing a box around the corrupted signal. Write down the labels of poor-quality channels.

▲ CRITICAL STEP Identifying poor-quality channels is important for avoiding the contamination of other channels during remontaging in Step 41.

```
cfg = [];
cfg.viewmode = 'vertical';
cfg = ft_databrowser(cfg, data);
```

40 Remove any poor-quality segments marked in the above step using the command below.

```
data = ft_rejectartifact(cfg, data);
```

41 Using the code below, remontage the cortical grids to a common average reference in order to remove noise that is shared across all channels.

```
cfg = [];
cfg.channel = {'LPG*', 'LTG*'};
cfg.reref = 'yes';
cfg.refchannel = 'all';
cfg.refmethod = 'avg';
reref_grids = ft_preprocessing(cfg, data);
```

Box 4 provides background information on remontaging. Poor-quality channels identified in Step 39 can be excluded from this step by adding those channels to cfg.channel with a minus prefix. That is, use cfg.channel = {'LPG*', 'LTG*', '-LPG1'} to exclude the LPG1 channel from the list of LPG and LTG channels.

Box 4 | Remontaging

The recorded electrophysiological signals are a mixture of the signal-of-interest and noise, both neural and non-neural. The main objective of the preprocessing of the neural recordings is to improve the signal-to-noise ratio of the data while optimally preparing it for follow-up analysis. Remontaging to a different referencing scheme, also known as a montage, may aid in the removal of noise that is shared across multiple channels. The common average re-referencing technique, for instance, involves taking the average potential from all channels and subtracting this global noise estimate from the potential in each channel[49,71-74]. We demonstrated how to apply this technique to the cortical grid electrodes in our example case.

Depth electrodes, located inside the brain and using differently sized and shaped contact points, have a different sensitivity distribution and capture different types of activity and levels of noise[2]. Currently, no consensus exists on the preferred montage for depth-electrode recordings and, thus, which electrodes to use as references[75-78]. White-matter signals may not be as silent as one would intuitively expect, and bipolar signals, despite being relatively clean, miss out on activity that had the same amplitude on the two consecutive electrodes before their combination[5,79]. Different options may need to be tested and evaluated per case, taking into account the purpose of any follow-up analysis[73]. For instance, see ref. [57] for a discussion of connectivity analysis in relation to the referencing scheme.

42 Apply a bipolar montage to the depth electrodes. This can be done by repeating Step 41 but selecting single-channel labels for `cfg.channel` and `cfg.refchannel`. Alternatively, it can be done using the code below, containing `cfg.refmethod = 'bipolar'`, which automatically takes bipolar derivations of consecutive channels.

```
depths = {'RAM*', 'RHH*', 'RTH*', 'ROC*', 'LAM*', 'LHH*', 'LTH*'};
for d = 1:numel(depths)
cfg = [];
cfg.channel = ft_channelselection(depths{d}, data.label);
cfg.reref = 'yes';
cfg.refchannel = 'all';
cfg.refmethod = 'bipolar';
cfg.updatesens = 'yes';
reref_depths{d} = ft_preprocessing(cfg, data);
end
```

New channel labels in the output indicate the bipolar origin of the data, e.g., 'RAM1–RAM2', 'RAM2–RAM3', and so on. By specifying `cfg.updatesens = 'yes'`, the same bipolar montage is automatically applied to the channel positions, with the resulting *chanpos* field containing the mean locations of all electrode pairs that constitute a bipolar channel. More elaborate schemes can be created by the specification of weight matrices using `cfg.montage` that define how existing channels should be combined into new channels (type `help ft_apply_montage` for further guidance).

43 Combine the data from both electrode types into one data structure for the ease of further processing using the code below.

```
cfg = [];
cfg.appendsens = 'yes';
reref = ft_appenddata(cfg, reref_grids, reref_depths{:});
```

44 Using the command below, save the re-referenced data to a file.

```
save([subjID '_reref.mat'], reref);
```

(Optional) Time–frequency analysis ● Timing ~2 min

45 Decompose the signal in time and frequency using time-resolved Fourier-based spectral decomposition. The below command samples the neural activity using `cfg.toi` throughout the 300-ms baseline period before tone onset at 0 ms and until after the approximate button-press time at 700 ms. At each time point, the spectral content is estimated using 200-ms windows (`cfg.t_ftimwin`) for a broad range of frequencies specified with `cfg.foi`.

```
cfg = [];
cfg.method = 'mtmconvol';
cfg.toi = -.3:0.01:.8;
cfg.t_ftimwin = ones(length(cfg.foi),1).*0.2;
cfg.foi = 5:5:200;
cfg.taper = 'hanning';
cfg.output = 'pow';
cfg.keeptrials = 'no';
freq = ft_freqanalysis(cfg, reref);
```

The settings for spectral decomposition depend on the clinical or research question at hand and contingencies in the experimental paradigm. Given that task-related changes in high-frequency-band activity (70–150 Hz) are the focus of this analysis, relatively short time windows of 200 ms are used. This time window imposes a frequency resolution of 5 Hz, given that it fits only integer multiples of that frequency's cycle. The 200-ms time window captures 20 cycles of a 100-Hz rhythm, which is well over the three cycles minimally required to unambiguously recover the spectral information. To reliably capture lower frequencies, the length of the time window may need to be increased, data-segment length permitting. Finally, note that `cfg.keeptrials` is set to 'no' (as it is by default), which results in the average spectral content across all trials being returned (type `help ft_freqanalysis` for further guidance).

46 Using the command below, save the time–frequency data to a file.

```
save([subjID '_freq.mat'], 'freq');
```
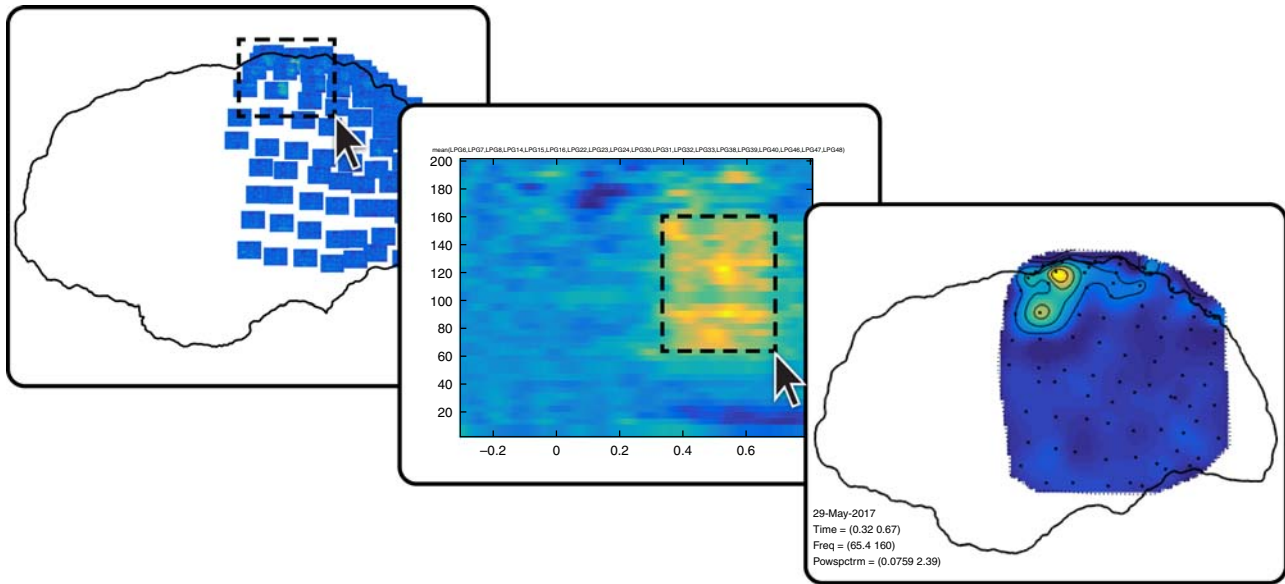
Fig. 5 | Interactive plotting. Fast browsing through various anatomically informed representations of the neural data can help address the multidimensionality of intracranial EEG data. Selecting a group of channels in the main figure on the left will launch another figure representing the average time–frequency representation over those channels (middle). Selecting a certain frequency and time range in that time–frequency representation will launch yet another figure showing the topographical distribution of activity in the selected interval (right), and so on.

Interactive plotting ● Timing ~3 min

47 For an anatomically informed exploration of the multidimensional outcome of an analysis, create a layout based on the 3D electrode locations, using the command below.

```
cfg = [];
cfg.headshape = pial_lh;
cfg.projection = 'orthographic';
cfg.channel = {'LPG*', 'LTG*'};
cfg.viewpoint = 'left';
cfg.mask = 'convex';
cfg.boxchannel = {'LTG30', 'LTG31'};
lay = ft_prepare_layout(cfg, freq);
```

This layout is a symbolic representation in which the channels are projected on the 2D medium offered by paper or a computer screen. The layout is complemented by an automatic outline of the cortical sheet that is specified in `cfg.headshape` the command. The `cfg.boxchannel` option allows selection of channels whose 2D distances are used to determine the plotting box sizes in the following step.

48 Using the command below, express the time–frequency representation of neural activity at each channel in terms of the relative change in activity from the baseline interval. The baseline interval from –100 to 0 ms is excluded, given that power spectral data points in this interval were estimated using 200-ms time windows that extend into the task period.

```
cfg = [];
cfg.baseline = [-.3 -.1];
cfg.baselinetype = 'relchange';
freq_blc = ft_freqbaseline(cfg, freq);
```

49 Using the command below, visualize the time–frequency representations overlaid on the 2D layout.

```
cfg = [];
cfg.layout = lay;
cfg.showoutline = 'yes';
ft_multiplotTFR(cfg, freq_blc);
```

The generated figure is interactive, so that selecting a group of channels will launch another figure representing the average time–frequency representation over those channels (Fig. 5). Selecting a certain frequency and time range in that time–frequency representation will launch yet another
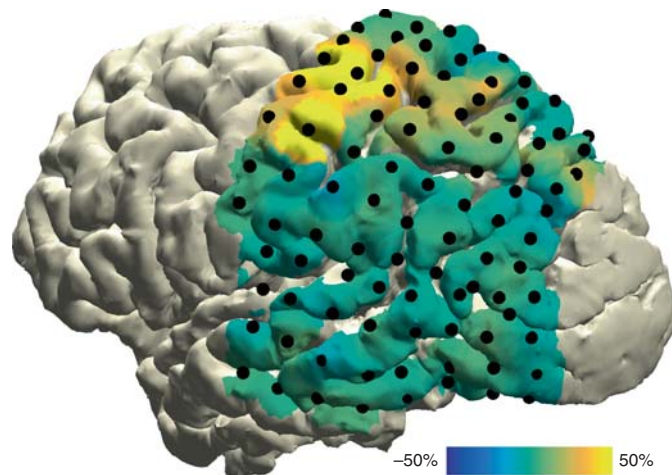
Fig. 6 | ECoG data representation obtained from the example dataset. Task-induced high-frequency-band activity (70–150 Hz) relative to a baseline interval, plotted on a cortical surface mesh of the subject's brain. The neural activity is averaged across the frequency band of interest and the time interval between 0 and 800 ms following the onset of a tone that required the subject to prepare and execute a button press with the right hand. The spatiotemporal dynamics of high-frequency-band activity time-locked to tone and button press can be observed in Supplementary Video 6.

figure showing the topographical distribution of activity in the selected interval, and so on (see also Supplementary Video 5 for guidance).

ECoG data representation ● Timing ~1 min

50 For an anatomically realistic representation of cortical activity, overlay a surface model of the neocortex with the spatial distribution of high-frequency-band activity. First, extract mean high-frequency-band activity during a time interval of interest with the command below.

```
cfg = [];
cfg.frequency = [70 150];
cfg.avgoverfreq = 'yes';
cfg.latency = [0 0.8];
cfg.avgovertime = 'yes';
freq_sel = ft_selectdata(cfg, freq_blc);
```

51 Using the command below, visualize the spatial distribution of high-frequency-band activity on a cortical mesh of the subject's brain (Fig. 6).

```
cfg = [];
cfg.funparameter = 'powspctrm';
cfg.funcolorlim = [-.5 .5];
cfg.method = 'surface';
cfg.interpmethod = 'sphere_weighteddistance';
cfg.sphereradius = 8;
cfg.camlight = 'no';
ft_sourceplot(cfg, freq_sel, pial_lh);
view([-90 20]);
material dull;
lighting gouraud;
camlight;
```

By repeating Step 50 and this step with the time interval of interest specified with `cfg.latency` broken down in consecutive steps, the spatiotemporal dynamics of neural activity occurring in relation to known experimental structure and behavior can be observed (see Supplementary Video 6 for an example of results obtained from using the example dataset). Type `help getframe` for capturing and assembling time-lapse movies.

52 Using the command below, add the electrodes to the figure.

```
ft_plot_sens(elec_acpc_fr);
```

SEEG data representation ● Timing ~2 min

53 For depth recordings, create an integrated representation of neural activity and anatomy by interpolating neural data from each bipolar channel in a spherical cloud, which can then be overlaid on a surface mesh of any deep-brain structure. First, create a volumetric mask of the regions of interest. The command below generates a mask for the right hippocampus and amygdala from the cortical parcellation and subcortical segmentation produced by FreeSurfer.

```
atlas = ft_read_atlas('freesurfer/mri/aparc+aseg.mgz');
atlas.coordsys = 'acpc';
cfg = [];
cfg.inputcoord = 'acpc';
cfg.atlas = atlas;
cfg.roi = {'Right-Hippocampus', 'Right-Amygdala'};
mask_rha = ft_volumelookup(cfg, atlas);
```

54 Using the command below, create a triangulated and smoothed surface mesh on the basis of the volumetric masks.

```
seg = keepfields(atlas, {'dim', 'unit','coordsys','transform'});
seg.brain = mask_rha;
cfg = [];
cfg.method = 'iso2mesh';
cfg.radbound = 2;
cfg.maxsurf = 0;
cfg.tissue = 'brain';
cfg.numvertices = 1000;
cfg.smooth = 3;
mesh_rha = ft_prepare_mesh(cfg, seg);
```

55 Using the command below, identify the subcortical electrodes of interest.

```
cfg = [];
cfg.channel = {'RAM*', 'RTH*', 'RHH*'};
freq_sel2 = ft_selectdata(cfg, freq_sel);
```
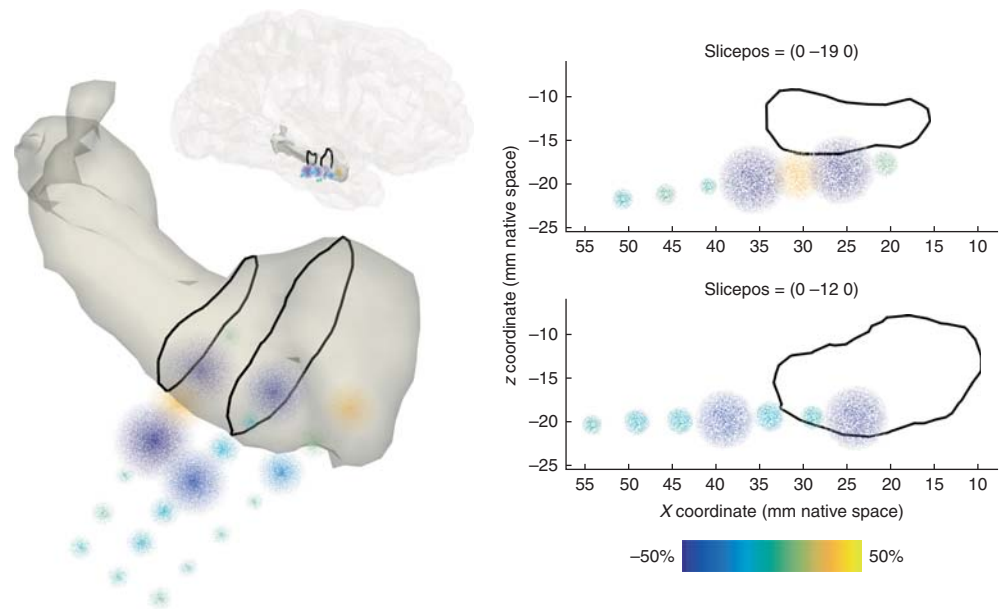

Fig. 7 | SEEG data representation. Task-induced high-frequency-band activity (70–150 Hz) relative to a baseline interval, plotted as point clouds around a triangulated mesh of a different subject's right amygdala and hippocampus combined. The neural activity is averaged across the frequency band of interest and the time interval between 0 and 800 ms following the onset of a tone that required the subject to prepare and execute a button press with the right hand. The size and color of the point clouds are scaled according to the percentage of high-gamma-band activity modulation from baseline power. The 2D planes on the right correspond to the slices indicated by the black lines in the image on the left.

56 Using the commands below, interpolate the high-frequency-band activity in the bipolar channels on a spherical cloud around the channel positions while overlaying the neural activity with the above mesh. (Supplementary Figure 1 shows examples of the cloud types currently available to plot.)

```
cfg = [];
cfg.funparameter = 'powspctrm';
cfg.funcolorlim = [-.5 .5];
cfg.method = 'cloud';
cfg.slice = '3d';
cfg.nslices = 2;
cfg.facealpha = .25;
ft_sourceplot(cfg, freq_sel2, mesh_rha);
view([120 40]);
lighting gouraud;
camlight;
```

By repeating the above command for neural data corresponding to consecutive time intervals, similar to the process outlined in Step 51, it becomes feasible to create time-lapse movies of the spatiotemporal dynamics of deep-brain activity. (Supplementary Video 7 shows the spatiotemporal evolution of epileptiform activity obtained from a dataset from a different subject.)

57 To create a more definitive image of the neural activity at particular positions, use the command below to generate 2D slices through the 3D representations. This combination provides the most complete and integrated representation of neural and anatomical data (Fig. 7).

```
cfg.slice = '2d';
ft_sourceplot(cfg, freq_sel2, mesh_rha);
```

Troubleshooting

Troubleshooting advice can be found in Table 1.

Table 1 | Troubleshooting table

Step	Problem	Possible reason	Solution
7	Unsatisfactory quality of cortical surfaces	Insufficient quality of the MRI	Repeat Step 6 on another MRI or manually correct the topological defects (see FreeSurfer website)
14	Severe misalignment of CT and MRI	Failure of the automatic CT conversion in Step 12	Use educated guesses of the commissure locations to directly align to the ACPC system in Step 11
	Imperfect alignment of CT and MRI	A left–right flip of either the MRI or the CT	Re-examine the native orientations of the MRI and CT in Steps 3 and 10, and redo the preprocessing of the affected scan
	Imperfect alignment of CT and MRI	MRI and CT contain different head anatomies	Repeat Step 13 with a different cost function (type *help ft_volumerealign*)
17	Electrodes are hard to identify in the 2D orthogonal plot	Cortical grid orientation is not aligned with any of the 2D planes	Identify electrodes in the 3D scatter figure (check the scatter checkbox)
19	Electrodes are missing or mislabeled	Human error during electrode placement	Revisit Step 17 to correct while specifying *cfg.elec = elec_acpc_f* to include previously localized electrodes
24	Severe deformation of the electrode grid	Incorrect pairing of neighboring electrodes in space	Repeat Step 23 with alternative settings (type *help ft_electroderealign*)
28	Severe displacement of electrodes	Insufficient quality of the MRI	Repeat Step 26 with an alternative cost function or template version (type *help ft_volumenormalise*)
34	No anatomical label found	No overlap of electrode position with any anatomical mask	Increase the search radius around the electrode by increasing the *cfg.maxqueryrange* value (type *help ft_volumelookup*)

Timing

Step 1, specification of subject ID: ~1 min
Steps 2–5, preprocessing of the anatomical MRI: ~2 min
Steps 6–8, (optional) cortical surface extraction with FreeSurfer: ~10 h
Steps 9–12, preprocessing of the anatomical CT: ~2 min
Steps 13–15, fusion of the CT with the MRI: ~3 min

Steps 16–20, electrode placement: ~15 min
Steps 21–25, (optional) brain-shift compensation: ~5 min
Steps 26–29, (optional) volume-based registration: ~2 min
Steps 30–32, (optional) surface-based registration: ~2 min
Steps 33 and 34, (optional) anatomical labeling: ~1 min
Steps 35–44, preprocessing of the neural recordings: ~10 min
Steps 45 and 46, (optional) time–frequency analysis: ~2 min
Steps 47–49, interactive plotting: ~3 min
Steps 50–52, ECoG data representation: ~1 min
Steps 53–57, SEEG data representation: ~2 min
Box 1, getting started with FieldTrip: ~1 min
Box 2, example data set
Box 3, coordinate system determination: ~1 min
Box 4, remontaging

Anticipated results

Upon completion of the protocol, an integrated representation of neural and anatomical data should be obtained. The exact results ultimately depend on the clinical or research question at hand, contingencies in the experimental paradigm, and decisions made during the execution of the protocol. For example, the worked example we provide here demonstrates the spatiotemporal neural dynamics that occur in relation to known experimental structure and relatively simple behavior, specifically the pressing of a button with the right hand when hearing a target tone (results obtained from the example dataset are shown in Figs. 5–7 and Supplementary Video 6). However, with small adaptations of the protocol, it is feasible to track the spatiotemporal evolution of epileptiform activity with high precision (e.g., Supplementary Video 7) or to perform group-level investigations of fine-grained emotion- or language-related neural dynamics in the human hippocampus[20,24]. A precise fusion of the anatomical images with the electrophysiological data is key to reproducible analyses and findings. Hence, it is important to examine the outcome of each part of the analysis as described in the Procedure and illustrated by Figs. 3 and 4.

Further information on experimental design is available in the **Life Sciences Reporting Summary**.

References

1. Buzsaki, G., Anastassiou, C. A. & Koch, C. The origin of extracellular fields and currents--EEG, ECoG, LFP and spikes. *Nat. Rev. Neurosci.* **13**, 407–420 (2012).
2. Malmivuo, J. & Plonsey, R. *Bioelectromagnetism: Principles and Applications of Bioelectric and Biomagnetic Fields. Bioelectromagnetism: Principles and Applications of Bioelectric and Biomagnetic Fields* (Oxford University Press, New York, 2012).
3. Brunner, P. et al. A practical procedure for real-time functional mapping of eloquent cortex using electro-corticographic signals in humans. *Epilepsy Behav.* **15**, 278–286 (2009).
4. Ritaccio, A. et al. Proceedings of the fifth international workshop on advances in electrocorticography. *Epilepsy Behav.* **41**, 183–92 (2014)
5. Lachaux, J.-P., Axmacher, N., Mormann, F., Halgren, E. & Crone, N. E. High-frequency neural activity and human cognition: past, present and possible future of intracranial EEG research. *Prog. Neurobiol.* **98**, 279–301 (2012).
6. Friston, J. A. & Friston, K. Multimodal image coregistration and partitioning - a unified fFramework. *Neuroimage* 6, 209–217 (1997).
7. Jenkinson, M., Bannister, P., Brady, M. & Smith, S. Improved optimization for the robust and accurate linear registration and motion correction of brain images. *Neuroimage* **17**, 825–841 (2002).
8. Cox, R. W. AFNI: software for analysis and visualization of functional magnetic resonance neuroimages. *Comput. Biomed. Res.* **29**, 162–73 (1996).
9. Papademetris, X. et al. BioImage suite: an integrated medical image analysis suite: an update. *Insight J.* **2006**, 209 (2006).
10. Azarion, A. A. et al. An open-source automated platform for three-dimensional visualization of subdural electrodes using CT-MRI coregistration. *Epilepsia* **55**, 2028–2037 (2014).
11. Blenkmann, A. O. et al. iElectrodes: a comprehensive open-source Toolbox for depth and subdural grid electrode localization. *Front. Neuroinform.* **11**, 14 (2017).

12. Groppe, D. M. et al. iELVis: an open source MATLAB toolbox for localizing and visualizing human intra-cranial electrode data. *J. Neurosci. Methods* **281**, 40–48 (2017).

13. Kubanek, J. & Schalk, G. NeuralAct: a tool to visualize electrocortical (ECoG) activity on a three-dimensional model of the cortex. *Neuroinformatics* **13**, 167–174 (2015).

14. Qin, C. et al. Automatic and precise localization and cortical labeling of subdural and depth intracranial electrodes. *Front. Neuroinform.* **11**, 1–10 (2017).

15. Hill, N. J. et al. Recording human electrocorticographic (ECoG) signals for neuroscientific research and real-time functional cortical mapping. *J. Vis. Exp.* https://doi.org/10.3791/3993(2012).

16. LaPlante, R. A. et al. The interactive electrode localization utility: software for automatic sorting and labeling of intracranial subdural electrodes. *Int. J. Comput. Assist. Radiol. Surg.* **12**, 1829–1837 (2017).

17. Branco, M. P. et al. ALICE: a tool for automatic localization of intra-cranial electrodes for clinical and high-density grids. *J. Neurosci. Methods* **301**, 43–51 (2018).

18. Eglen, S. J. et al. Toward standard practices for sharing computer code and programs in neuroscience. *Nat. Neurosci.* **20**, 770–773 (2017).

19. Delorme, A. & Makeig, S. EEGLAB: an open source toolbox for analysis of single-trial EEG dynamics including independent component analysis. *J. Neurosci. Methods* **134**, 9–21 (2004).

20. Zheng, J. et al. Amygdala-hippocampal dynamics during salient information processing. *Nat. Commun.* **8**, 14413 (2017).

21. Tang, C., Hamilton, L. S. & Chang, E. F. Intonational speech prosody encoding in the human auditory cortex. *Science* **357**, 797–801 (2017).

22. Martinet, L.-E. et al. Human seizures couple across spatial scales through travelling wave dynamics. *Nat. Commun.* **8**, 14896 (2017).

23. Gelinas, J. N., Khodagholy, D., Thesen, T., Devinsky, O. & Buzsáki, G. Interictal epileptiform discharges induce hippocampal–cortical coupling in temporal lobe epilepsy. *Nat. Med.* **22**, 641–648 (2016).

24. Piai, V. et al. Direct brain recordings reveal hippocampal rhythm underpinnings of language processing. *Proc. Natl Acad. Sci. USA* **113**, 11366–11371 (2016).

25. Hermes, D., Miller, K. J., Noordmans, H. J., Vansteensel, M. J. & Ramsey, N. F. Automated electro-corticographic electrode localization on individually rendered brain surfaces. *J. Neurosci. Methods* **185**, 293–298 (2010).

26. Dalal, S. S. et al. Localization of neurosurgically implanted electrodes via photograph-MRI-radiograph coregistration. *J. Neurosci. Methods* **174**, 106–115 (2008).

27. Yang, A. I. et al. Localization of dense intracranial electrode arrays using magnetic resonance imaging. *Neuroimage* **63**, 157–165 (2012).

28. Onofrey, J. A., Staib, L. H. & Papademetris, X. Learning intervention-induced deformations for non-rigid MR-CT registration and electrode localization in epilepsy patients. *NeuroImage Clin.* **10**, 291–301 (2016).

29. Pieters, T. A., Conner, C. R. & Tandon, N. Recursive grid partitioning on a cortical surface model: an optimized technique for the localization of implanted subdural electrodes. *J. Neurosurg.* **118**, 1086–1097 (2013).

30. Stieglitz, L. H. et al. Improved localization of implanted subdural electrode contacts on magnetic resonance imaging with an elastic image fusion algorithm in an invasive electroencephalography recording. *Clin. Neurosurg.* **10**, 506–513 (2014).

31. Brang, D., Dai, Z., Zheng, W. & Towle, V. L. Registering imaged ECoG electrodes to human cortex: a geometry-based technique. *J. Neurosci. Methods* **273**, 64–73 (2016).

32. Dykstra, A. R. et al. Individualized localization and cortical surface-based registration of intracranial electrodes. *Neuroimage* **59**, 3563–3570 (2012).

33. Khodagholy, D. et al. Organic electronics for high-resolution electrocorticography of the human brain. *Sci. Adv.* **2**, 1–9 (2016).

34. Seo, D. et al. Wireless recording in the peripheral nervous system with ultrasonic neural dust. *Neuron* **91**, 529–539 (2016).

35. Lauro, P. M. et al. DBSproc: an open source process for DBS electrode localization and tractographic analysis. *Hum. Brain Mapp.* **37**, 422–433 (2016).

36. Horn, A. & Kühn, A. A. Lead-DBS: a toolbox for deep brain stimulation electrode localizations and visualizations. *Neuroimage* **107**, 127–135 (2015).

37. Dale, A. M., Fischl, B. & Sereno, M. I. Cortical surface-based analysis: I. Segmentation and surface reconstruction. *Neuroimage* **9**, 179–194 (1999).

38. Lepore, N. et al. A new combined surface and volume registration. *Med. Imaging 2010 Image Process.* **7623**, 76231E https://doi.org/10.1117/12.844434(2010).

39. Klein, A. et al. Evaluation of volume-based and surface-based brain image registration methods. *Neuroimage* **51**, 214–220 (2010).

40. Hill, D. L. G. et al. Measurement of intraoperative brain surface deformation under a craniotomy. *Neurosurgery* **43**, 514–526 (1998).

41. Roberts, D. W., Hartov, A., Kennedy, F. E., Miga, M. I. & Paulsen, K. D. Intraoperative brain shift and deformation: a quantitative analysis of cortical displacement in 28 cases. *Neurosurgery* **43**, 749–758 (1998).

42. Miyagi, Y., Shima, F. & Sasaki, T. Brain shift: an error factor during implantation of deep brain stimulation electrodes. *J. Neurosurg.* **107**, 989–97 (2007).

43. Hastreiter, P. et al. Strategies for brain shift evaluation. *Med. Image Anal.* **8**, 447–464 (2004).

44. LaViolette, P. S. et al. Three-dimensional visualization of subdural electrodes for presurgical planning. *Oper. Neurosurg.* **68** https://doi.org/10.1227/NEU.0b013e31820783ba (2011).

45. Sweet, J. A., Hdeib, A. M., Sloan, A. & Miller, J. P. Depths and grids in brain tumors: Implantation strategies, techniques, and complications. *Epilepsia* **54**, 66–71 (2013).

46. Kovalev, D. et al. Rapid and fully automated visualization of subdural electrodes in the presurgical evaluation of epilepsy patients. *Am. J. Neuroradiol.* **26**, 1078–1083 (2005).

47. Wang, P. T. et al. A co-registration approach for electrocorticogram electrode localization using post-implantation MRI and CT of the head. in *Proc. International. IEEE/EMBS Conference on Neural Engineering, NER* 525–528 https://doi.org/10.1109/NER.2013.6695987(2013).

48. Schulze-Bonhage, A. H. J. et al. Visualization of subdural strip and grid electrodes using curvilinear reformatting of 3D MR imaging data sets. *Am. J. Neuroradiol.* **23**, 400–403 (2002).

49. Boatman-Reich, D. et al. Quantifying auditory event-related responses in multichannel human intracranial recordings. *Front. Comput. Neurosci.* **4**, 4 (2010).

50. Staresina, B. P. et al. Hierarchical nesting of slow oscillations, spindles and ripples in the human hippocampus during sleep. *Nat. Neurosci.* **18**, 1679–1686 (2015).

51. Manning, J. R., Jacobs, J., Fried, I. & Kahana, M. J. Broadband shifts in local field potential power spectra are correlated with single-neuron spiking in humans. *J. Neurosci.* **29**, 13613–13620 (2009).

52. Miller, K. J. Broadband spectral change: evidence for a macroscale correlate of population firing rate? *J. Neurosci.* **30**, 6477–6479 (2010).

53. Ray, S. & Maunsell, J. H. R. Different origins of gamma rhythm and high-gamma activity in macaque visual cortex. *PLoS Biol.* **9** https://doi.org/10.1371/journal.pbio.1000610 (2011).

54. Crone, N. E., Miglioretti, D. L., Gordon, B., Lesser, R. P. & Crone, N. Functional mapping of human sensorimotor cortex with electrocorticographic spectral analysis II. Event-related synchronization in the gamma band. *Brain* **121**, 2301–2315 (1998).

55. Oostenveld, R., Fries, P., Maris, E. & Schoffelen, J. M. FieldTrip: open source software for advanced analysis of MEG, EEG, and invasive electrophysiological data. *Comput. Intell. Neurosci.* **2011** https://doi.org/10.1155/2011/156869 (2011).

56. Maris, E. & Oostenveld, R. Nonparametric statistical testing of EEG- and MEG-data. *J. Neurosci. Methods* **164**, 177–190 (2007).

57. Bastos, A. M. & Schoffelen, J.-M. A tutorial review of functional connectivity analysis methods and their interpretational pitfalls. *Front. Syst. Neurosci.* **9**, 1–23 (2016).

58. Drury, H. A., Van Essen, D. C., Corbetta, M. & Snyder, A. Z. *Brain Warping* 337–363 (Elsevier, Cambridge, MA, 1999).

59. Wells, W. M., Viola, P., Atsumi, H., Nakajima, S. & Kikinis, R. Multi-modal volume registration by maximization of mutual information. *Med. Image Anal.* **1**, 35–51 (1996).

60. Collignon, A. & Maes, F. Automated multi-modality image registration based on information theory. *Proc. Inf. Process. Med. Imaging* 263–274 (1995).

61. Schaer, M. et al. A surface-based approach to quantify local cortical gyrification. *IEEE Trans. Med. Imaging* **27**, 161–170 (2008).

62. Lancaster, J. L. et al. Automated labeling of the human brain: a preliminary report on the development and evaluation of a forward-transform method. *Hum. Brain Mapp.* **5**, 238–242 (1997).

63. Tzourio-Mazoyer, N. et al. Automated anatomical labeling of activations in SPM using a macroscopic anatomical parcellation of the MNI MRI single-subject brain. *Neuroimage* **15**, 273–289 (2002).

64. Cocosco, C. A., Kollokian, V., Kwan, R. K., Pike, G. B. & Evans, A. C. BrainWeb: online interface to a 3D MRI simulated brain database. *Proc. 3rd Int. Conf. Funct. Mapp. Hum. Brain* **5**, S425 (1997). in.

65. Eickhoff, S. B. et al. A new SPM toolbox for combining probabilistic cytoarchitectonic maps and functional imaging data. *Neuroimage* **25**, 1325–1335 (2005).

66. Wang, L., Mruczek, R. E. B., Arcaro, M. J. & Kastner, S. Probabilistic maps of visual topography in human cortex. *Cereb. Cortex* **25**, 3911–3931 (2015).

67. Fan, L. et al. The human brainnetome atlas: a new brain atlas based on connectional architecture. *Cereb. Cortex* **26**, 3508–3526 (2016).

68. Desikan, R. S. et al. An automated labeling system for subdividing the human cerebral cortex on MRI scans into gyral based regions of interest. *Neuroimage* **31**, 968–980 (2006).

69. Destrieux, C., Fischl, B., Dale, A. & Halgren, E. Automatic parcellation of human cortical gyri and sulci using standard anatomical nomenclature. *Neuroimage* **53**, 1–15 (2010).

70. Ashburner, J. & Friston, K. J. Nonlinear spatial normalization using basis functions. *Hum. Brain Mapp.* **7**, 254–266 (1999).

71. Bigdely-Shamlo, N., Mullen, T., Kothe, C., Su, K.-M. & Robbins, K. A. The PREP pipeline: standardized preprocessing for large-scale EEG analysis. *Front. Neuroinform.* **9**, 16 (2015).

72. Liu, Y., Coon, W. G., Pesters, A., de Brunner, P. & Schalk, G. The effects of spatial filtering and artifacts on electrocorticographic signals. *J. Neural Eng.* **12**, 56008 (2015).

73. Dien, J. Issues in the application of the average reference: review, critiques, and recommendations. *Behav. Res. Methods, Instrum., Comput.* **30**, 34–43 (1998).

74. Ludwig, K. A. et al. Using a common average reference to improve cortical neuron recordings from microelectrode arrays. *J. Neurophysiol.* **101**, 1679–1689 (2009).

75. Trongnetrpunya, A. et al. Assessing Granger causality in electrophysiological data: removing the adverse effects of common signals via bipolar derivations. *Front. Syst. Neurosci.* **9**, 189 (2015).
76. Shirhatti, V., Borthakur, A. & Ray, S. Effect of reference scheme on power and phase of the local field potential. *Neural Comput.* 882–913 https://doi.org/10.1162/NECO (2016).
77. Arnulfo, G., Hirvonen, J., Nobili, L., Palva, S. & Palva, J. M. Phase and amplitude correlations in resting-state activity in human stereotactical EEG recordings. *Neuroimage* **112**, 114–127 (2015).
78. Zaveri, H. P., Duckrow, R. B. & Spencer, S. S. On the use of bipolar montages for time-series analysis of intracranial electroencephalograms. *Clin. Neurophysiol.* **117**, 2102–2108 (2006).
79. Mercier, M. R. et al. Evaluation of cortical local field potential diffusion in stereotactic electro-encephalography recordings: a glimpse on white matter signal. *Neuroimage* **147**, 219–232 (2017).

Acknowledgements

Author contributions

A.S., S.G., R.v.d.M., J.-M.S., and R.O. developed the protocol. G.P. contributed the algorithm for brain-shift compensation. J.J.L. provided access and guidance in the data acquisition. A.S., S.G., J.-M.S., R.T.K., and R.O. wrote the paper, and R.v.d.M., C.D., I.S., G.P., and J.J.L., provided substantial editorial revisions.

Competing interests

The authors declare no competing interests.

Additional information

Supplementary information is available for this paper at https://doi.org/10.1038/s41596-018-0009-6.

Reprints and permission information is available online at www.nature.com/reprints

Correspondence and requests for materials should be addressed to A.S.

Publisher's note: Springer Nature remains neutral with regard to jurisdictional claims in published maps and institutional affiliations.

Published online: 09 July 2018

Related links

1. Zheng, J. et al. *Nat. Commun.* **8**, 14413 (2017): http://dx.doi.org/10.1038/ncomms14413
2. Piai et al. *Proc. Natl. Acad. Sci. USA* **113**, 11366–11371 (2016): http://dx.doi.org/10.1073/pnas.1603312113